Available online at www.sciencedirect.com
SCIENCE DIRECT®
Journal of Magnetic Resonance 168 (2004) 88–96
JMR Journal of Magnetic Resonance
www.elsevier.com/locate/jmr

Hyperfine decoupling in electron paramagnetic resonance as a powerful tool for unraveling complicated ESEEM spectra of $S = 1/2$, $I \geqslant 1/2$ systems

George Mitrikas and Arthur Schweiger*

Physical Chemistry Laboratory, Swiss Federal Institute of Technology, CH-8093 Zurich, Switzerland

Received 15 November 2003; revised 26 January 2004

Abstract

Hyperfine decoupling in electron paramagnetic resonance after strong microwave radiation is studied for $S = 1/2$, $I = 1/2$ and $S = 1/2$, $I = 1$ spin systems. A new 2D pulse sequence based on the hyperfine-decoupled DEFENCE (deadtime-free ESEEM by nuclear coherence-transfer echoes) experiment is introduced, which is distinguished by a remarkable reduction of the residual hyperfine coupling. The efficiency of this new decoupling experiment in comparison to the old pulse sequence is studied by means of numerical simulations. The advantages of the new decoupling experiment and its ability to simplify ESEEM spectra are experimentally demonstrated on two disordered systems.

Keywords: Hyperfine-decoupling; ESEEM frequencies; Quadrupolar nuclei

1. Introduction

Hyperfine decoupling in electron paramagnetic resonance (EPR) spectroscopy is based on well-established concepts used in nuclear magnetic resonance (NMR), for eliminating nuclear spin dipole–dipole and scalar interactions [1–3]. In NMR, usually transitions of one type of nuclear spins are irradiated and thereby decoupled from other type of nuclear spins which is detected. The main difference between decoupling in EPR and NMR is that in the former case the gyromagnetic ratios γ_i of the hyperfine-coupled electron and nuclear spins differ by two to three orders of magnitude. Since for an efficient hyperfine decoupling in EPR, the decoupling microwave (mw) or radiofrequency (RF) strength $\gamma_i B_1$ has to be larger than the hyperfine coupling, it is obvious that decoupling of electron spins from nuclear spins through mw radiation is relatively easy, whereas decoupling through RF radiation is virtually impossible. For this reason, in EPR hyperfine decoupling is only possible by exciting the electron spins which are also detected.

Recently, several hyperfine decoupling schemes have been developed [4–6]. In all these experiments the ongoing effort is towards resolution enhancement by using two-dimensional (2D) decoupling schemes that are based on three- and four-pulse electron spin echo envelope modulation (ESEEM) experiments. The decoupled DEFENCE (deadtime-free ESEEM by nuclear coherence (NC)-transfer echoes) pulse sequence has been found to be a powerful 2D experiment, especially for the case of orientationally disordered $S = 1/2, I = 1/2$ spin systems.

Apart from the question of the efficiency of hyperfine decoupling under strong mw radiation [7], the main motivation for the development of hyperfine decoupling experiments arises from their ability to simplify complicated spectra of $S = 1/2$, $I > 1/2$ spin systems. This later issue is still a challenge for ESEEM spectroscopy, which during the last two decades has become an important experimental tool for determining weak hyperfine and quadrupole interactions [8,9]. The main complication in systems with nuclear spins $I > 1/2$ is caused by the quadrupole interaction that increases the number of the unknown parameters. This may cause

* Corresponding author. Fax: +41-1-632-15-38.
E-mail address: schweiger@esr.phys.chem.ethz.ch (A. Schweiger).

1090-7807/$ - see front matter © 2004 Elsevier Inc. All rights reserved.
doi:10.1016/j.jmr.2004.02.001

ambiguities in the determination of the magnetic parameters, even in cases where a non-linear least squares fitting of narrow features in ESEEM spectra is applicable [10]. Moreover, in disordered systems the anisotropic hyperfine and quadrupole interactions cause line-broadenings that make an interpretation of the spectra possible only via numerical simulations [11]. This issue becomes very demanding for systems with more than one interacting nucleus and/or with nuclear spins $I > 1$ [12–14]. The simplification of such complicated spectra has been the subject of numerous studies, including exact cancellation techniques [15,16] and high-field EPR [17]. However, these approaches can either not cover a broad range of hyperfine couplings or are technically very demanding.

In this work hyperfine decoupling is proposed as a way for simplifying ESEEM spectra. First, the theory for $S = 1/2$, $I = 1/2$ spin systems under strong mw radiation is extended to the case of $S = 1/2$, $I = 1$. The efficiency of the decoupled DEFENCE experiment is studied for these two systems by means of numerical simulations. A modified version of this pulse sequence is introduced, resulting in a virtually complete elimination of the residual hyperfine couplings for the first time. Finally, the advantages of this experiment and its ability to simplify ESEEM spectra are experimentally demonstrated on two disordered systems.

2. Theory

During hyperfine decoupling under strong resonant mw radiation the quantization axis of the nuclear spin I in a system of a coupled electron spin S and nuclear spin I remains unchanged, whereas the quantization axis of the electron spins is rotating with the Larmor frequency in the xy plane of the laboratory frame. The local field at nuclear spin I generated by the electron spin S thus becomes strongly time-dependent and is averaged for times $t \gg 2\pi/\omega_S$. In principle it is then possible to decouple the electron from the nuclear spin by applying a prolonged strong mw pulse. However, this simplified picture is not complete because for off-resonant spin packets there will still be a non-zero component of S along $\boldsymbol{B}_0$, resulting in a residual hyperfine coupling.

The aim of this theoretical study of hyperfine decoupling is to predict the nuclear frequencies of a spin system under strong mw radiation. For an $S = 1/2$, $I = 1/2$ spin system with an isotropic g value and an anisotropic hyperfine interaction with the nucleus in the xz plane of the laboratory frame, the rotating frame spin Hamiltonian including the radiation field along y can be written as [7]

$$\mathcal{H} = \mathcal{H}_0 + \omega_1 S_y = \Omega_S S_z + \omega_I I_z + A S_z I_z + B S_z I_x + \omega_1 S_y, \tag{1}$$

where $\Omega_S = (\omega_S - \omega_{\mathrm{mw}})$ is the resonance off-set of the electron Zeeman frequency $\omega_S = g\beta_e B_0/\hbar$ from the mw frequency ω_{mw}, $\omega_I = -g_n\beta_n B_0/\hbar$ is the nuclear Zeeman frequency, A and B describe the secular and pseudo-secular part of the hyperfine coupling, and $\omega_1 = g\beta_e B_1/\hbar$ is the mw field strength in angular frequency units. In the case of axially symmetric hyperfine interaction the coefficients A and B are given by [8] $A = a_{\mathrm{iso}} + T(3\cos^2\theta - 1)$ and $B = 3T\sin\theta\cos\theta$, where a_{iso} and T are the isotropic and dipolar part of the hyperfine coupling and θ is the polar angle defining the position of the nucleus in the xz plane. By expanding the eigenvalues of the Hamiltonian in Eq. (1) in a Taylor series at $1/\omega_1 = 0$, and neglecting terms of higher than second order we find for the decoupled nuclear frequencies in the two electron spin manifolds [7]

$$\omega_{\alpha,\beta}^{\mathrm{dec}} = \omega_I \pm \frac{A\Omega_S}{2\omega_1} - \frac{B^2(\Omega_S^2 - \omega_I^2)}{8\omega_1^2\omega_I}. \tag{2}$$

The frequencies in Eq. (2) are a good approximation for strong mw fields with $\omega_1 \gg (\Omega_S, \omega_I, A, B)$. This is illustrated in Fig. 1, where the exact solutions using numerical diagonalization are compared to the decoupled frequencies of Eq. (2).

The residual hyperfine splitting is given by

$$A_{\mathrm{res}} = \frac{A\Omega_S}{\omega_1} \tag{3}$$

and in the case of complete decoupling, or for on-resonant spin packets ($\Omega_S \approx 0$), the nuclear frequencies $\omega_{\alpha,\beta}^{\mathrm{dec}}$ approach the nuclear Zeeman frequency, $\omega_{\alpha,\beta}^{\mathrm{dec}} = \omega_I$, since also the non-secular contribution of $B^2\omega_I/8\omega_1^2$ becomes negligible for sufficiently strong mw fields.

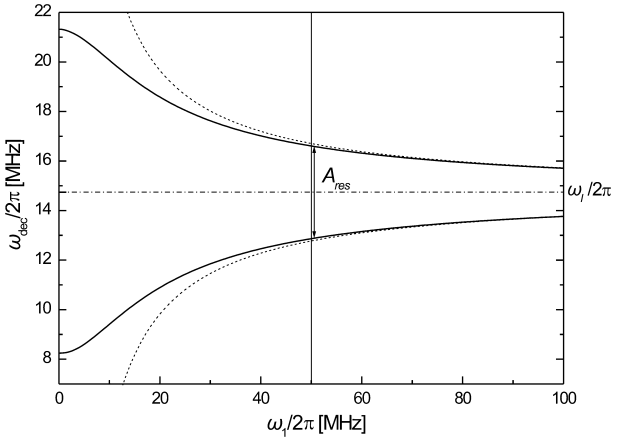

Fig. 1. Nuclear frequencies as a function of the decoupling field strength ω_1 for an $S = 1/2$, $I = 1/2$ spin system. Solid lines: exact solution for $\omega_\alpha^{\mathrm{dec}}$, $\omega_\beta^{\mathrm{dec}}$ obtained from numerical diagonalization of the Hamiltonian in Eq. (1). Dashed lines: nuclear frequencies predicted by Eq. (2). The residual hyperfine coupling for $\omega_1/2\pi = 50$ MHz is marked by an arrow. Parameters: nuclear Zeeman frequency, $\omega_I/2\pi = 14.7$ MHz; hyperfine couplings, $A/2\pi = 13.1$ MHz, and $B/2\pi = 2.1$ MHz; resonance offset, $\Omega_S/2\pi = 15$ MHz.

In the case of an $S = 1/2$, $I = 1$ system, the rotating frame spin Hamiltonian during mw radiation along y is given by

$$\begin{aligned}\mathcal{H} &= \mathcal{H}_0 + \omega_1 S_y \\ &= \Omega_S S_z + \omega_I I_z + A_z S_z I_z + B_x S_z I_x + B_y S_z I_y + \mathbf{IPI} + \omega_1 S_y.\end{aligned} \tag{4}$$

P is the nuclear quadrupole tensor which in its principal axes system is defined by

$$\mathbf{P}^d = \begin{pmatrix} -K(1-\eta) & & \\ & -K(1+\eta) & \\ & & 2K \end{pmatrix}, \tag{5}$$

where $K = e^2qQ/4\hbar$ represents the nuclear quadrupole coupling constant and η is the asymmetry parameter of the electric field gradient.

The diagonalization of the spin Hamiltonian in Eq. (4) and the expansion of the eigenvalues in a Taylor series in the limit $\omega_1 \to \infty$ becomes now rather tedious. An alternative approach, which is followed in the present study, is to find approximate solutions using second-order perturbation theory. More specifically, assuming a strong mw field, $\omega_1 \gg (\Omega_S, \omega_I, A, B_{x,y}, K)$, and a weak hyperfine and quadrupole coupling, $\omega_I > (A/2, K)$, we can treat the term $\omega_1 S_x + \omega_I I_z$ as the dominating part of the Hamiltonian and the remaining terms as perturbations. For the decoupled nuclear frequencies we then find:

$$\begin{aligned}\omega^{\mathrm{dec}}_{\mathrm{SQ1}(\alpha,\beta)} &= \omega_{\mathrm{SQ1}} \pm \frac{A\Omega_S}{2\omega_1} \pm \frac{A^2}{4\omega_1} + \frac{B^2}{8(\omega_I \mp \omega_1)}, \\ \omega^{\mathrm{dec}}_{\mathrm{SQ2}(\alpha,\beta)} &= \omega_{\mathrm{SQ2}} \pm \frac{A\Omega_S}{2\omega_1} \mp \frac{A^2}{4\omega_1} + \frac{B^2}{8(\omega_I \pm \omega_1)}, \\ \omega^{\mathrm{dec}}_{\mathrm{DQ}(\alpha,\beta)} &= \omega_{\mathrm{DQ}} \pm \frac{A\Omega_S}{\omega_1} + \frac{B^2\omega_I}{4(\omega_I^2 - \omega_1^2)},\end{aligned} \tag{6}$$

where the subscripts SQ1 and SQ2 denote the two single-quantum nuclear spin transitions $(m_I,\ m_I + 1) = (0, 1)$ and $(-1, 0)$, and DQ the double-quantum transition, $(-1, 1)$. The expressions:

$$\begin{aligned}\omega_{\mathrm{SQ1}} &= \omega_I + \frac{3}{2}P_{zz} + \frac{1}{2\omega_I}(P_{xy}^2 + P_{xz}^2 + P_{yz}^2) \\ &\quad + \frac{1}{8\omega_I}(P_{xx} - P_{yy})^2 + \mathrm{O}(3) \\ \omega_{\mathrm{SQ2}} &= \omega_I - \frac{3}{2}P_{zz} + \frac{1}{2\omega_I}(P_{xy}^2 + P_{xz}^2 + P_{yz}^2) \\ &\quad + \frac{1}{8\omega_I}(P_{xx} - P_{yy})^2 + \mathrm{O}(3), \\ \omega_{\mathrm{DQ}} &= 2\omega_I + \frac{1}{\omega_I}(P_{xy}^2 + P_{xz}^2 + P_{yz}^2) \\ &\quad + \frac{1}{4\omega_I}(P_{xx} - P_{yy})^2 + \mathrm{O}(3),\end{aligned} \tag{7}$$

denote the corresponding nuclear frequencies of the same spin system but with *zero* hyperfine coupling, obtained from the eigenvalues of the Hamiltonian $\mathcal{H}_{\mathrm{n}} = \Omega_S S_z + \omega_I I_z + \mathbf{IPI}$, and O(3) stands for higher than second-order terms. From Eq. (6) it can be seen that for very strong decoupling fields ($\omega_1 \to \infty$) the nuclear frequencies approach those given in Eq. (7), corresponding to complete decoupling ($A = 0$).

An example of this behavior is shown in Fig. 2. However, as in the case of $I = 1/2$, there is a residual hyperfine splitting, given by:

$$\begin{aligned}A^{\mathrm{SQ1}}_{\mathrm{res}} &= \frac{A\Omega_S}{\omega_1} + \frac{A^2}{2\omega_1} - \frac{B^2\omega_1}{4(\omega_1^2 - \omega_I^2)}, \\ A^{\mathrm{SQ2}}_{\mathrm{res}} &= \frac{A\Omega_S}{\omega_1} - \frac{A^2}{2\omega_1} + \frac{B^2\omega_1}{4(\omega_1^2 - \omega_I^2)}, \\ A^{\mathrm{DQ}}_{\mathrm{res}} &= 2\frac{A\Omega_S}{\omega_1}.\end{aligned} \tag{8}$$

Although the formulas in Eqs. (6) and (8) are good approximations only in the case of weak couplings ($2\omega_I > A$), the conservation of the nuclear Zeeman and quadrupole interaction during decoupling is a general property that does not depend on the magnitude of the hyperfine coupling. In other words, Eq. (7) gives good approximations of the *completely* decoupled frequencies for all magnitudes of hyperfine couplings.

The analysis described above demonstrates that the residual hyperfine splitting is a crucial parameter for an accurate determination of the decoupled frequencies, since only with spin packets with small off-resonance frequencies ($\Omega_S \approx 0$) narrow peaks will be obtained in the decoupled dimension. On the other hand, the residual hyperfine splittings arising from off-resonance

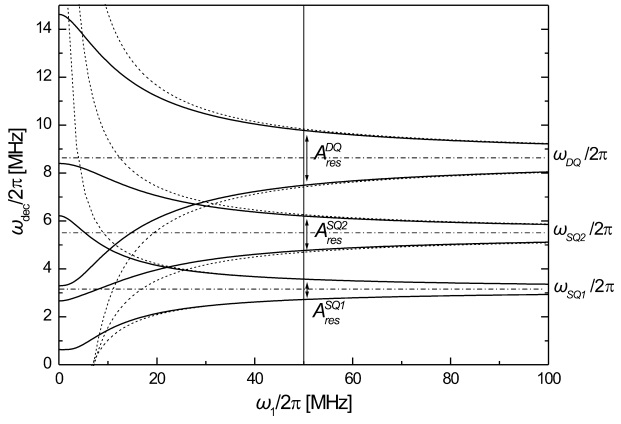

Fig. 2. Nuclear frequencies as a function of the decoupling field ω_1 for an $S = 1/2$, $I = 1$ spin system. Solid lines: exact solution for $\omega^{\mathrm{dec}}_{\mathrm{SQ1}(\alpha,\beta)}$, $\omega^{\mathrm{dec}}_{\mathrm{SQ2}(\alpha,\beta)}$, and $\omega^{\mathrm{dec}}_{\mathrm{DQ}(\alpha,\beta)}$ obtained from numerical diagonalization of the Hamiltonian in Eq. (4). Dashed lines: nuclear frequencies predicted by Eq. (6). The residual hyperfine couplings of the three nuclear spin transitions for $\omega_1/2\pi = 50$ MHz are marked by arrows. Decoupled frequencies: $\omega_{\mathrm{SQ1}}/2\pi = 3.15$ MHz, $\omega_{\mathrm{SQ2}}/2\pi = 5.48$ MHz, and $\omega_{\mathrm{DQ}}/2\pi = 8.63$ MHz (dotted-dashed lines). Parameters: nuclear Zeeman frequency, $\omega_I/2\pi = 4.19$ MHz; hyperfine couplings, $A/2\pi = -6.05$ MHz and $B/2\pi = -0.92$ MHz; nuclear quadrupole coupling, $P_{zz}/2\pi = 0.82$ MHz; resonance offset, $\Omega_S/2\pi = 10$ MHz.

spin packets scale with Ω_S/ω_1 and thus can only be reduced by applying sufficiently strong mw fields. However, since a typical maximum mw field is around $\omega_1/2\pi = 50\,\mathrm{MHz}$, complete decoupling is not possible with currently available commercial spectrometers. Therefore, new hyperfine decoupling schemes have to be used to eliminate residual hyperfine couplings.

3. Methods

3.1. Pulse sequences

Among the recently proposed hyperfine decoupling schemes [5,6], hyperfine-decoupled DEFENCE is the most promising approach. This scheme is based on the DEFENCE sequence [18], a 1D four-pulse ESEEM experiment which makes use of the sequence $\pi/2$–τ–$\pi/2$–t_1–π–t–$\pi/2$–τ-echo with a constant time t_1 and a variable time t. In the DEFENCE experiment, NC is created by the sub-sequence $\pi/2$–τ–$\pi/2$ and a NC-transfer echo is observed at about $t = t_1$. In the hyperfine-decoupled DEFENCE experiment, the third $\pi/2$ pulse is replaced by a decoupling pulse of variable length T_{dec} (Fig. 3A). This introduces a second dimension along which the hyperfine-decoupled frequencies can be obtained. In the original 1D-DEFENCE experiment, t_1 has to be long compared to T_{m} in order to separate the wanted NC-transfer echo from the unwanted FID and electron spin echoes. However, in the current decoupling experiment a choice of very long t_1 may result in a loss of sensitivity due to relaxation effects during the additional decoupling pulse. Nevertheless, the optimization of t_1 (by means of increase the ESEEM signal intensity) can be done by a trial and error variation of t_1 in the standard 1D DEFENCE experiment [18]. For the case of an $S = 1/2$, $I = 1/2$ spin system, the 2D decoupling experiment correlates the two nuclear frequencies $\omega_\alpha = \sqrt{(\omega_I + A/2)^2 + (B/2)^2}$ and $\omega_\beta = \sqrt{(\omega_I - A/2)^2 + (B/2)^2}$ with the corresponding decoupled frequency $\omega_{\mathrm{dec}} \approx \omega_I$, so that the nuclear frequency of different types of nuclei can be separated from each other.

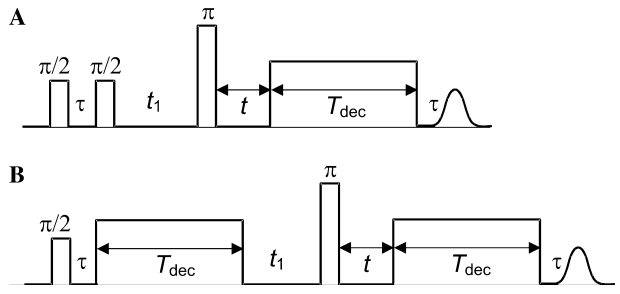

Fig. 3. Pulse sequences for hyperfine-decoupled ESEEM. (A) Hyperfine-decoupled DEFENCE. (B) New hyperfine-decoupled DEFENCE sequence.

The information from this 2D experiment is even more in demand for the $S = 1/2$, $I = 1$ case, where the six nuclear frequencies $\omega_{\mathrm{SQ1}(\alpha,\beta)}$, $\omega_{\mathrm{SQ2}(\alpha,\beta)}$, and $\omega_{\mathrm{DQ}(\alpha,\beta)}$ will be correlated with the corresponding decoupled frequencies given by Eq. (6), so that a direct determination of the nuclear quadrupole interaction becomes possible. However, the residual hyperfine splitting can still make the estimation of the decoupled frequencies difficult or even impossible. This is particularly true for $I = 1$ systems where, according to Eq. (8), even for resonant spin packets ($\Omega_S = 0$) a non-zero secular term contributes to the residual hyperfine spitting of the single-quantum nuclear spin transitions. In addition, the residual hyperfine splitting of the double-quantum transitions is two times larger than the one of the single-quantum transitions of the $I = 1/2$ system. The estimation of the decoupled frequencies for $I = 1$ systems is therefore more difficult than for the $I = 1/2$ case.

The residual splitting can be eliminated with the pulse sequence shown in Fig. 3B. In this 2D experiment which is based on the hyperfine-decoupled DEFENCE pulse sequence, the second $\pi/2$ pulse is replaced by a decoupling pulse of length T_{dec}. Again, the free evolution period t_1 is kept constant whereas the free evolution period t and the length T_{dec} of the two decoupling pulses are varied. In contrast to the previous pulse sequence, the nuclear coherence during the decoupling pulses evolves now in both electron spin manifolds. It is then expected, in analogy to the combination peak experiment [18] that also the frequencies $\omega_{\pm}^{\mathrm{dec}} = |\omega_\alpha^{\mathrm{dec}} \pm \omega_\beta^{\mathrm{dec}}|$ will appear in the decoupling dimension of the spectrum.

For the weak hyperfine coupling case ($2\omega_I > A$) with $I = 1/2$, for every off-resonance spin packet the decoupled frequencies $\omega_\alpha^{\mathrm{dec}}$, $\omega_\beta^{\mathrm{dec}}$ are in first order symmetrically placed around ω_I, so that the sum-combination frequency, $\omega_+^{\mathrm{dec}} = 2\omega_I$, is free from secular residual hyperfine contributions. Similarly, for $I = 1$, the six nuclear frequencies are correlated with the three sum-combination frequencies

$$\omega_{\mathrm{SQ1}(\alpha)}^{\mathrm{dec}} + \omega_{\mathrm{SQ1}(\beta)}^{\mathrm{dec}} = 2\omega_{\mathrm{SQ1}} - \frac{B^2\omega_I}{4\omega_1^2},$$

$$\omega_{\mathrm{SQ2}(\alpha)}^{\mathrm{dec}} + \omega_{\mathrm{SQ2}(\beta)}^{\mathrm{dec}} = 2\omega_{\mathrm{SQ2}} - \frac{B^2\omega_I}{4\omega_1^2},$$

and

$$\omega_{\mathrm{DQ}(\alpha)}^{\mathrm{dec}} + \omega_{\mathrm{DQ}(\beta)}^{\mathrm{dec}} = 2\omega_{\mathrm{DQ}} - \frac{B^2\omega_I}{2\omega_1^2}.$$

For sufficiently strong mw fields the shifting terms containing the non-secular hyperfine coupling B can be neglected and the sum-combination frequencies become twice the *completely* decoupled frequencies given in Eq. (7). Finally, for both nuclear spins $I = 1/2$ and $I = 1$, the nuclear frequencies will also be correlated with ω_-^{dec},

which is equal to the residual hyperfine splitting given in Eqs. (3) and (8), respectively.

For a further comparison of the efficiency of the two hyperfine-decoupling experiments analytical formulas are required. However, they are quite tedious and only few insights can be gained from them. An alternative approach, followed in this work, is to demonstrate the basic features of the frequency correlation patterns using numerical simulations of the corresponding experiments.

3.2. Numerical simulations

The numerical simulations were performed in time domain using the product operator formalism [8,11]. The pulses were treated as ideal except the decoupling pulses. For the decoupling pulses the propagator $R_{\mathrm{dec}} = \exp(-\mathrm{i}\mathcal{H}T_{\mathrm{dec}})$ was used, where $\mathcal{H}$ is the spin Hamiltonian during decoupling given in Eqs. (1) and (4) for the $I = 1/2$ and $I = 1$ systems.

The calculations of the 2D time-domain spectra were carried out with a program written in MATLAB 6.0 (The MathWorks, Natick, MA). The usual eight-step phase cycle was applied to eliminate unwanted electron coherences. A resonance-offset integration was performed assuming a Gaussian distribution. Finally, the calculated time-domain data were baseline corrected with a constant, apodized with a Hamming window and zero filled. After 2D Fourier transformation, the absolute-value spectra were calculated.

The simulated frequency correlation patterns for an $S = 1/2$, $I = 1/2$ spin system with $\nu_I = 14.7\,\mathrm{MHz}$, $A/2\pi = 13.1\,\mathrm{MHz}$, and $B/2\pi = 2.1\,\mathrm{MHz}$ are shown in Fig. 4. For the decoupled DEFENCE experiment (Fig. 4A), the two nuclear frequencies $\nu_\alpha = 8.2\,\mathrm{MHz}$ and $\nu_\beta = 21.3\,\mathrm{MHz}$ in the ESEEM dimension are correlated with symmetrically disposed frequencies around ν_I in the decoupling dimension. This simulation demonstrates how the effect of the residual hyperfine coupling results in an elongation of the correlation peaks along the decoupling dimension and thus makes an estimation of $\nu_{\alpha,\beta}^{\mathrm{dec}} \approx \nu_I$ uncertain. Fig. 4B shows the simulated spectrum of the same system using the new pulse sequence. The nuclear frequencies ν_α, ν_β in the ESEEM dimension are now also

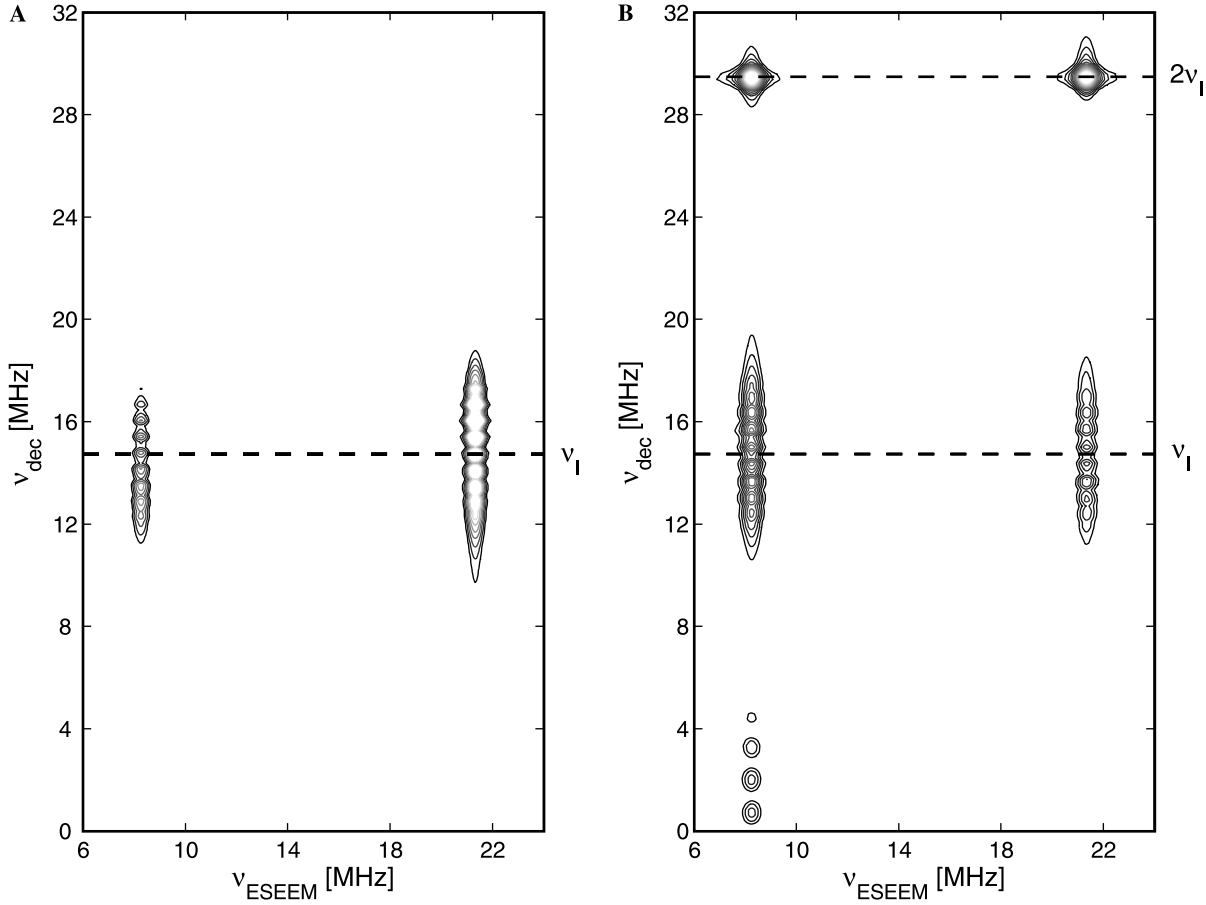

Fig. 4. Numerical computations of hyperfine decoupling experiments for an $S = 1/2$, $I = 1/2$ spin system. (A) Hyperfine-decoupled DEFENCE. (B) New hyperfine-decoupled DEFENCE sequence. Parameters: nuclear Zeeman frequency, $\nu_I = 14.7\,\mathrm{MHz}$; hyperfine couplings, $A/2\pi = 13.1\,\mathrm{MHz}$ and $B/2\pi = 2.1\,\mathrm{MHz}$. Decoupling field, $\omega_1/2\pi = 50\,\mathrm{MHz}$; $\tau = 100\,\mathrm{ns}$; $t_1 = 96\,\mathrm{ns}$; starting values for t and T_{dec} 16 ns varied in steps of $\Delta t = 16\,\mathrm{ns}$, $\Delta T_{\mathrm{dec}} = 4\,\mathrm{ns}$ (150×600 data points); an inhomogeneous broadening is assumed with a Gaussian line shape of $(\Delta\Omega_{\mathrm{S}})_{\mathrm{FWHH}}/2\pi = 15\,\mathrm{MHz}$.

correlated with the frequency $\nu_{\alpha,\beta}^{\mathrm{dec}} \approx 2\nu_I$ in the decoupling dimension. The sum-combination frequency thus results in a remarkable reduction of the residual hyperfine splitting in the decoupling dimension. Moreover, low-intensity correlation peaks between ν_α and the residual hyperfine coupling frequencies are observed.

The corresponding numerical simulations for an $S = 1/2$, $I = 1$ spin system were carried out assuming an axially symmetric hyperfine interaction with the parameters $\nu_I = 4.19\,\mathrm{MHz}$, $a_{\mathrm{iso}}/2\pi = -6.70\,\mathrm{MHz}$, $T/2\pi = 0.65\,\mathrm{MHz}$, $K/2\pi = 0.62\,\mathrm{MHz}$, and $\eta = 0.88$, where a_{iso} and T are the isotropic and anisotropic part of the hyperfine coupling. The orientations of the principal axes systems of the hyperfine and nuclear quadrupole tensors with respect to the static magnetic field $\boldsymbol{B}_0$ are defined by the Euler angles ($\alpha_{\mathrm{H}} = 0°$, $\beta_{\mathrm{H}} = 35.4°$, and $\gamma_{\mathrm{H}} = 0°$) and ($\alpha_{\mathrm{Q}} = 0°$, $\beta_{\mathrm{Q}} = 34.6°$, and $\gamma_{\mathrm{Q}} = 0°$). For this specific orientations, the secular and pseudo-secular parts of the hyperfine coupling are $A/2\pi = -6.05\,\mathrm{MHz}$ and $B/2\pi = -0.92\,\mathrm{MHz}$, whereas the P_{zz} element of the nuclear quadrupole tensor is $P_{zz}/2\pi = 0.82\,\mathrm{MHz}$. The above parameters reproduce the basic features of the correlation pattern obtained for $VO(acac)_2$/pyridine at Q-band (see Section 5). The numerical diagonalization of $\mathcal{H}_0$ with these parameters results in the six nuclear frequencies $\nu_{\mathrm{SQ1}(\alpha)} = 6.22\,\mathrm{MHz}$, $\nu_{\mathrm{SQ2}(\alpha)} = 8.40\,\mathrm{MHz}$, $\nu_{\mathrm{DQ}(\alpha)} = 14.62\,\mathrm{MHz}$, and $\nu_{\mathrm{SQ1}(\beta)} = 0.63\,\mathrm{MHz}$, $\nu_{\mathrm{SQ2}(\beta)} = 2.66\,\mathrm{MHz}$, $\nu_{\mathrm{DQ}(\beta)} = 3.29\,\mathrm{MHz}$. The simulation of the decoupled DEFENCE experiment is shown in Fig. 5A. The dashed lines denote the nuclear frequencies in the limit of *complete* hyperfine decoupling with $\nu_{\mathrm{SQ1}} = 3.15\,\mathrm{MHz}$, $\nu_{\mathrm{SQ2}} = 5.48\,\mathrm{MHz}$, and $\nu_{\mathrm{DQ}} = 8.63\,\mathrm{MHz}$.

The elongation of the correlation peaks in the decoupling dimension is again pronounced. Only the decoupled frequencies corresponding to the double-quantum correlation peaks are roughly symmetrically arranged with respect to ν_{DQ}. For the two single-quantum ESEEM frequencies, $\nu_{\mathrm{SQ1}(\alpha)}$ and $\nu_{\mathrm{SQ1}(\beta)}$, the decoupled frequencies are lower than ν_{SQ1}. This residual hyperfine splitting, observed even for on-resonance spin packets, makes an estimation of the decoupled frequencies uncertain for systems with $I = 1$, in accordance with Eq. (8).

The 2D pattern obtained with the new decoupled DEFENCE experiment is shown in Fig. 5B. The additional correlation of the nuclear frequencies with twice the decoupled frequencies results again in a remarkable reduction of the residual hyperfine splitting in the decoupling dimension. Consequently, this new decoupling scheme allows the direct determination of the nuclear quadrupole interactions.

4. Experimental

The experiments were performed on polycrystalline bis(*n*-benzene) vanadium(0), $V(bz)_2$, diluted into

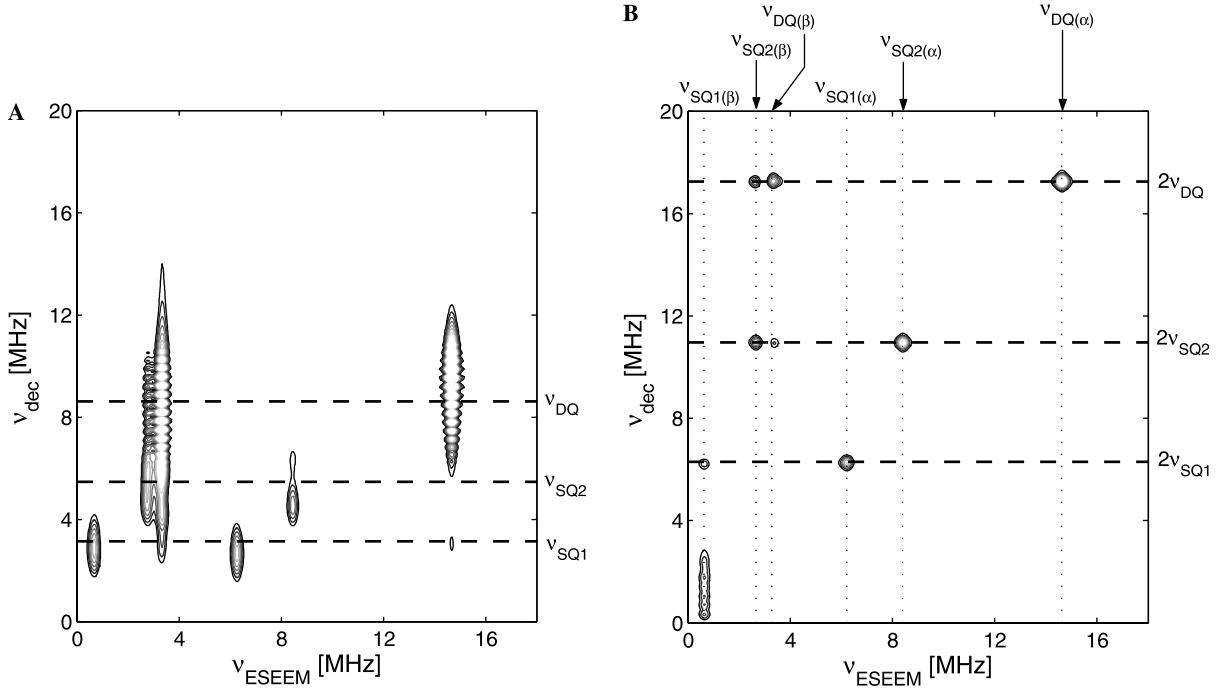

Fig. 5. Numerical computations of hyperfine decoupling experiments for an $S = 1/2$, $I = 1$ spin system. (A) Hyperfine-decoupled DEFENCE. (B) New hyperfine-decoupled DEFENCE sequence. Parameters: nuclear Zeeman frequency, $\nu = 4.19\,\mathrm{MHz}$; hyperfine couplings, $A/2\pi = -6.05\,\mathrm{MHz}$ and $B/2\pi = -0.92\,\mathrm{MHz}$; nuclear quadrupole coupling, $P_{zz}/2\pi = 0.82\,\mathrm{MHz}$; decoupling field, $\omega_1/2\pi = 50\,\mathrm{MHz}$; $\tau = 170\,\mathrm{ns}$; $t_1 = 160\,\mathrm{ns}$; starting values for t and T_{dec} 16 ns varied in steps of $\Delta t = 16\,\mathrm{ns}$, $\Delta T_{\mathrm{dec}} = 8\,\mathrm{ns}$ (300×600 data points); an inhomogeneous broadening is assumed with a Gaussian line shape of $(\Delta\Omega_S)_{\mathrm{FWHH}}/2\pi = 20\,\mathrm{MHz}$.

ferrocene, 1:100 [19] and on bis(acetylacetonato)oxovanadium(IV)/pyridine, $VO(acac)_2$/pyridine [20]. $VO(acac)_2$/pyridine was prepared by dissolving $VO(acac)_2$ (0.02 M) and pyridine (0.04 M) in a mixture of $CHCl_3$/toluene (1:1). The solution was then transferred to an EPR tube and degassed using the usual freeze–pump–thaw method.

The experiments on $V(bz)_2$ were carried out on a Bruker Elexsys E580 spectrometer (X-band, mw frequency 9.69 GHz) equipped with an EN4118 probe head. The experiments on $VO(acac)_2$/pyridine were performed on a home-built Q-band instrument (mw frequency 35.3 GHz) [21]. The mw conversion factor of the resonator was approximately $2.5\,G/\sqrt{W}$ for Q factors between 100 and 300. All experiments were carried out at a temperature of 40 K with a helium gas-flow cryogenic system from Oxford Instruments, with a repetition rate of 1 kHz. During the decoupling pulses, the mw field strength was $\omega_1/2\pi \approx 32$ MHz. The length of the decoupling pulses was varied in steps of $\Delta T_{dec} = 8$ ns starting from $T_0 = 16$ ns. The following experimental conditions were used: $t_{\pi/2} = 16$ ns, $t_\pi = 16$ ns, $\Delta t = 8$ ns starting from $t_0 = 96$ ns, $t_1 = 160$ ns, $\tau = 120$ ns ($V(bz)_2$), and 170 ns ($VO(acac)_2$/pyridine); an eight-step phase cycle was used.

The data were processed with the program MATLAB 6.0 (The MathWorks, Natick, MA). The time traces were baseline corrected with a third-order polynomial, apodized with a Hamming window and zero filled. After 2D Fourier transformation, the absolute-value spectra were calculated.

5. Experimental examples and discussion

The results obtained with the two hyperfine-decoupling sequences on $V(bz)_2$ at X-band are shown in Fig. 6. Both experiments were performed at an arbitrary observer position ($B_0 = 344.3$ mT). In the hyperfine-decoupled DEFENCE spectrum (Fig. 6A) strong correlation peaks are observed in the decoupling dimension around the nuclear proton Larmor frequency $\nu_H = 14.7$ MHz. The broad peaks with maximum intensities around 10 and 19.3 MHz along the ESEEM dimension represent the protons of the benzene rings. In addition, ^{13}C cross-peaks in natural abundance between the ESEEM frequencies 3.1 and 4.9 MHz and the ^{13}C Larmor frequency $\nu_C = 3.7$ MHz in the decoupling dimension are observed. The effect of the residual proton hyperfine coupling is evident, since the correlation frequencies in the decoupling dimension deviate considerably from the corresponding nuclear Larmor frequencies.

The results obtained with the new pulse sequence are shown in Fig. 6B. The spectrum contains now additional correlation peaks, which are very narrow along the decoupling dimension at $2\nu_H = 29.4$ MHz and $2\nu_C = 7.4$ MHz. The residual hyperfine couplings are

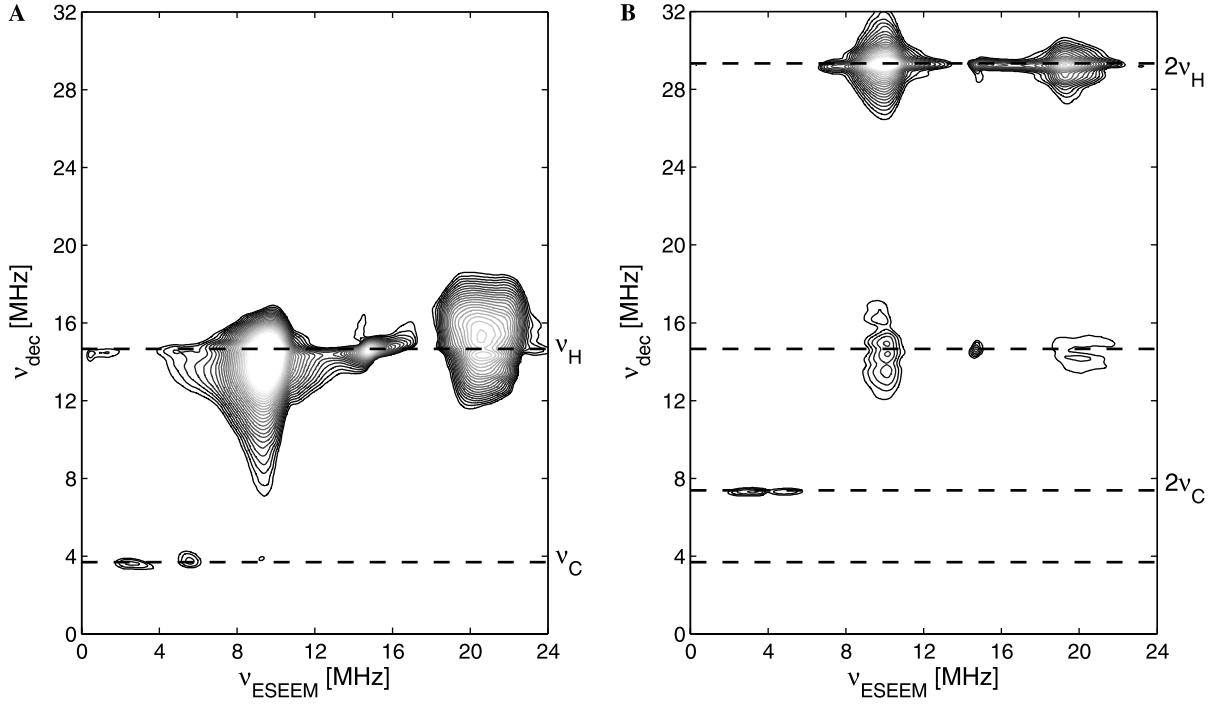

Fig. 6. Hyperfine decoupling experiments on polycrystalline bis(*n*-benzene)vanadium(0) at X-band. Experimental parameters: arbitrary observer position; mw field strength of decoupling pulses, $\omega_1/2\pi \approx 32$ MHz; $\tau = 120$ ns; $t_1 = 160$ ns; starting value for t, $t_0 = 96$ ns varied in steps of $\Delta t = 8$ ns; starting value for T_{dec}, $T_0 = 16$ ns varied in steps of $\Delta T_{dec} = 8$ ns (500×500 data points); number of accumulations, $N = 6$. (A) Hyperfine-decoupled DEFENCE. (B) New hyperfine-decoupled DEFENCE sequence.

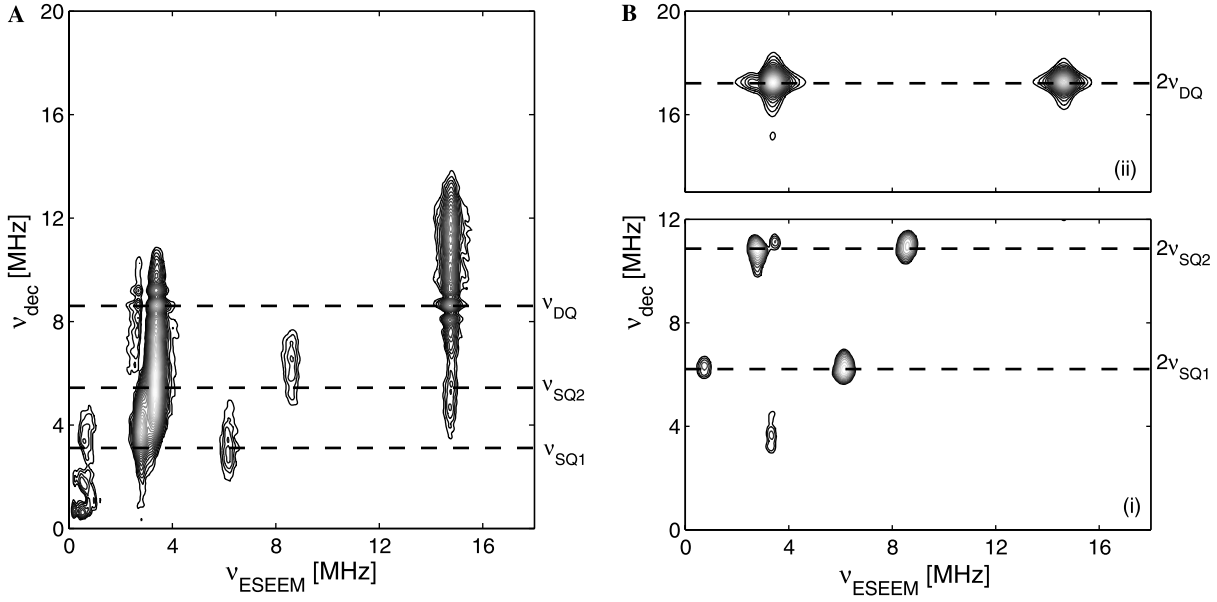

Fig. 7. Hyperfine decoupling experiments on bis(acetylacetonato)oxovanadium(IV)/pyridine in a frozen $CHCl_3$/toluene (1:1) solution at Q-band. Experimental parameters: observer position, $g_{\|}$; mw field strength of decoupling pulses, $\omega_1/2\pi \approx 32$ MHz; $\tau = 170$ ns; $t_1 = 160$ ns; starting value for t, $t_0 = 96$ ns varied in steps of $\Delta t = 8$ ns; starting value for T_{dec}, $T_0 = 16$ ns varied in steps of $\Delta T_{dec} = 8$ ns (512×512 data points); number of accumulations, $N = 10$. (A) Hyperfine-decoupled DEFENCE. (B) New hyperfine-decoupled DEFENCE sequence; lowest contour levels: (i) 5% and (ii) 15% of the maximum peak intensity (double-quantum correlation peaks).

virtually eliminated in agreement with the simulations shown in Section 3.2.

The decoupling experiments on $VO(acac)_2$/pyridine at Q-band performed at the observer position $g_{\|}(B_0 = 1360.9\,\text{mT})$ are shown in Fig. 7. Strong interactions with the pyridine nitrogen ($\nu_N = 4.2$ MHz) are observed in both 2D plots. In the ESEEM dimension, the dominating peaks at $\nu_{DQ(\beta)} = 3.4$ and $\nu_{DQ(\alpha)} = 14.7$ MHz represent the double-quantum frequencies. The single-quantum frequencies $\nu_{SQ1(\beta)} = 0.7$, $\nu_{SQ2(\beta)} = 2.8$ and $\nu_{SQ1(\alpha)} = 6.2$, $\nu_{SQ2(\alpha)} = 8.6$ MHz are also observed. In the standard decoupled DEFENCE experiment, the effect of the residual hyperfine coupling results again in a broadening of the correlation peaks along the decoupling dimension (Fig. 7A) and the determination of the decoupled frequencies becomes uncertain.

The cancellation of the residual hyperfine coupling obtained with the new decoupling experiment is demonstrated in Fig. 7B. Narrow correlation peaks along the decoupling dimension appear at the frequencies 6.2, 10.9, and 17.2 MHz. These frequencies correspond to twice the decoupled frequencies $\nu_{SQ1} = 3.1$ MHz, $\nu_{SQ2} = 5.5$ MHz, and $\nu_{DQ} = 8.6$ MHz. With these frequencies and the expressions of Eq. (7), we find $\nu_{SQ2} - \nu_{SQ1} \approx 3P_{zz}/2\pi = 2.4$ MHz, and finally a nuclear quadrupole coupling of $P_{zz}/2\pi = 0.8$ MHz, which is in accordance with the value of 0.85 MHz estimated from ENDOR measurements [20]. The difference between $\nu_{DQ} = 8.6$ MHz and $2\nu_N = 8.4$ MHz is attributed to second- and higher-order contributions as denoted in Eq. (7).

Note that the expressions in Eq. (7), connecting the decoupled frequencies with the nuclear quadrupole parameters, are good approximations only when the nuclear Zeeman term is considerably larger than the nuclear quadrupole interaction, $\omega_I \gg K$. However, this is not generally the case. Consequently, a least-square fitting, based on a comparison between the experimentally determined decoupled frequencies and the exact solutions of the spin Hamiltonian $\mathcal{H}_n = \Omega_S S_z + \omega_I I_z + \mathbf{IPI}$, is by far more useful and accurate. Such a treatment is only possible with data obtained with the new pulse sequence, because the decoupled frequencies are free of hyperfine couplings.

As described before, the key-point of the new method is the symmetric position of the decoupled frequencies with respect to the *completely* decoupled ones (see Fig. 2 for example). This is true for the weak coupling case, $2\omega_I > A$. For the case of strong coupling, $2\omega_I < A$, the sum-combination frequencies still contain residual hyperfine coupling terms that are expected to cause a line broadening along the decoupling dimension. For $VO(acac)_2$/pyridine, the hyperfine coupling of the pyridine nitrogen is $A/2\pi \approx -6$ MHz and this justifies the particular choice of the Q-band mw frequency for the present study ($\nu_N = 4.2$ MHz). However, for systems with weak or intermediate hyperfine couplings at X-band mw frequencies, the method will also be successful.

A complete determination of the nuclear quadrupole data, including the asymmetry parameter η and the orientation of the principal axis system with respect to the molecular frame, is only possible from

measurements at different observer positions which is beyond the scope of this paper. However, as is concluded from the above discussion, the new hyperfine-decoupling experiment can simplify complicated ESEEM spectra in disordered systems and thus allows for a more straightforward determination of nuclear quadrupole parameters. Related studies on spin systems with $I > 1$ are currently in progress.

6. Conclusions

Hyperfine decoupling was examined as a tool for ESEEM spectra simplification, especially for systems with $I = 1$. A theoretical study of the nuclear frequencies during strong mw radiation showed that, for $I = 1$, a non-zero residual hyperfine coupling is present even for resonant spin packets. We therefore introduced a new 2D pulse sequence which is based on the decoupled DEFENCE experiment. The new experiment combines the advantage of an undistorted spectrum along the ESEEM dimension and a remarkable reduction of the residual hyperfine couplings along the decoupling dimension. This is verified by numerical simulations and experimental results, and allows for a more accurate determination of the nuclear quadrupole parameters compared to traditional ESEEM-based experiments. Hyperfine-decoupling experiments thus open a new way for unraveling complicated spectra of paramagnetic species with quadrupolar nuclei.

Acknowledgment

This research has been supported by the Swiss National Science Foundation.

References

[1] A. Abragam, The Principles of Nuclear Magnetism, Clarendon, Oxford, 1961.
[2] C.P. Slichter, Principles of Magnetic Resonance, third ed., Springer, Berlin, 1966.
[3] R.R. Ernst, G. Bodenhausen, A. Wokaum, Principles of NMR in One and Two Dimensions, Clarendon, Oxford, 1987.
[4] G. Jeschke, A. Schweiger, Basics and features of spin-locked electron spin echo envelope modulation, Chem. Phys. Lett. 231 (1994) 574–578.
[5] G. Jeschke, A. Schweiger, Hyperfine decoupling in electron spin resonance, J. Chem. Phys. 106 (1997) 9979–9991.
[6] S. Van Doorslaer, A. Schweiger, New hyperfine-decoupling schemes in electron paramagnetic resonance spectroscopy, Chem. Phys. Lett. 308 (1999) 187–194.
[7] G. Jeschke, A. Schweiger, Generation and transfer of coherence in electron–nuclear spin systems by non-ideal microwave pulses, Mol. Phys. 88 (1996) 355–383.
[8] A. Schweiger, G. Jeschke, Principles of Pulse Electron Paramagnetic Resonance, Oxford University Press, Oxford, 2001.
[9] Y. Deligiannakis, M. Louloudi, N. Hadjiliadis, Electron spin echo envelope modulation (ESEEM) spectroscopy as a tool to investigate the coordination environment of metal centers, Coord. Chem. Rev. 204 (2000) 1–112.
[10] E.J. Reijerse, A.M. Tyryshkin, S.A. Dikanov, Complete determination of nitrogen quadrupole and hyperfine tensors in an oxovanadium complex by simultaneous fitting of multifrequency ESEEM powder spectra, J. Magn. Reson. 131 (1998) 295–309.
[11] Z.L. Mádi, S. Van Doorslaer, A. Schweiger, Efficient simulation of ESEEM spectra, J. Magn. Reson. 154 (2002) 181–191.
[12] J. Harmer, S. Van Doorslaer, I. Gromov, A. Schweiger, Corrin nitrogens and remote dimethylbenzimidazole nitrogen interactions in Cob(II)alamin studied with HYSCORE at X- and Q-band, Chem. Phys. Lett. 358 (2002) 8–16.
[13] L. Astrakas, Y. Deligiannakis, G. Mitrikas, G. Kordas, Hyperfine sublevel correlation spectroscopy in lithium silicate glasses, J. Chem. Phys. 109 (1998) 8612–8616.
[14] M. Gutjahr, R. Böttcher, A. Pöppl, Analysis of correlation patterns in hyperfine sublevel correlation spectroscopy of $S = 1/2$, $I = 3/2$ systems, Appl. Magn. Reson. 22 (2002) 401–414.
[15] A. Lai, H.F. Flanagan, D.J. Singel, Multifrequency electron spin echo envelope modulation in $S = 1/2$, $I = 1/2$ systems: analysis of the spectral amplitudes, line shapes, and linewidths, J. Chem. Phys. 89 (1988) 7161–7166.
[16] H.L. Flanagan, D.J. Singel, Analysis of ^{14}N ESEEM patterns of randomly oriented solids, J. Chem. Phys. 87 (1987) 5606–5616.
[17] A. Bloess, K. Möbius, T.F. Prisner, High-frequency/high-field electron spin echo envelope modulation study of nitrogen hyperfine and quadrupole interactions on a disordered powder sample, J. Magn. Reson. 134 (1998) 30–35.
[18] A. Ponti, A. Schweiger, Nuclear coherence-transfer echoes in pulsed EPR, J. Chem. Phys. 102 (1995) 5207–5219.
[19] R. Wolf, A. Schweiger, Hs.H. Gunthard, ENDOR on vanadium D5-sandwich compounds. 1. Influence of the crystal-field symmetry on the magnetic parameters of dibenzene vanadium, Mol. Phys. 53 (1984) 567–583.
[20] B. Kirste, H. van Willigen, Electron nuclear double resonance study of bis(acetylacetonato)oxovanadium(IV) and some of its adducts in frozen solution, J. Chem. Phys. 86 (1982) 2743–2749.
[21] I. Gromov, J. Shane, J. Forrer, R. Rakhmatoullin, Yu. Rozentzwaig, A. Schweiger, A Q-band pulse EPR/ENDOR spectrometer and the implementation of advanced one- and two-dimensional pulse EPR methodology, J. Magn. Reson. 149 (2001) 196–203.